Modeling and experimental characterization of an active MEMS-based force sensor

Jonathan Cailliez, Mokrane Boudaoud, Abdenbi Mohand Ousaid, Antoine Duflos, Sinan Haliyo, Stéphane Regnier

Modeling and Experimental Characterization of an Active MEMS Based Force Sensor

Jonathan Cailliez, Mokrane Boudaoud, Abdenbi Mohand Ousaid, Antoine Weill–Duflos, Sinan Haliyo and Stéphane Régnier

***Abstract*— Active force sensors are based on the principle of force balancing using a feedback control. They allow, unlike passive sensors, the measurement of forces in a wide range with nanoNewton resolutions. This capability is fundamental when dealing with the mechanical characterization of samples with a wide range of stiffness. This paper deals with the modeling and the experimental characterization of a new active MEMS based force sensor. This sensor includes folded-flexure type suspensions and a differential comb drive actuation allowing a linear force/voltage relationship. A control oriented electromechanical model is proposed and validated experimentally in static and dynamic operating modes using a stroboscopic measurement system. The sensor has a resonant frequency of 2.2 kHz, and a static passive measurement range of ± 2.45 μN. This work is the first step toward new dynamic measuring capabilities and sensing at the micro/nano-scales when high dynamic, large measurement range and nanoNewton resolution are required.**

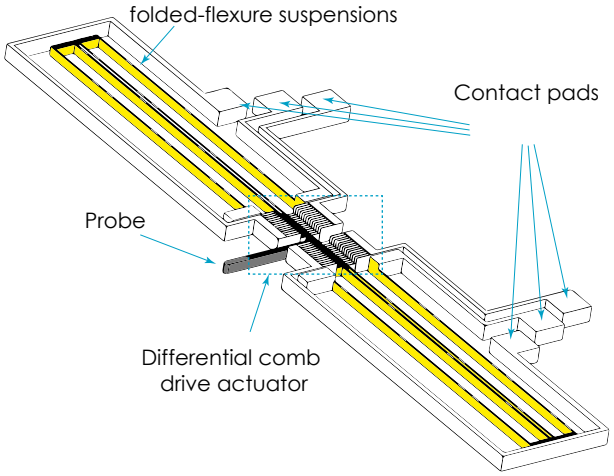

Fig. 1. 3D CAD view of the MEMS based for sensor. The folded-flexure suspensions are highlighted in yellow.

I. Introduction

Small and embeddable force sensing tools are essential in micro-robotics [1]. The need of size reduction has led to forgo traditional engineering techniques for sensors fabrication in favor of cleanroom fabrication processes. The cleanroom facilities have made possible the production of the well known Micro Electro Mechanical Systems (MEMS). MEMS engineering can provide systems with much smaller details [2] than conventional techniques and can perform batch manufacturing, efficiently reducing the cost and time of production.

MEMS force sensing can be divided into two main categories, namely elastic sensing and zero displacement sensing. The first one is the most widely reported in the literature with piezoresistive sensors [3][4], fluidic sensors [5], capacitive sensors [6][7], MOSFET sensors [8] and so on. In capacitive sensors, a mechanical structure is used to transform an external force into a displacement. The force measurement is deduced from the displacement measurement by the knowledge of mechanical suspensions stiffness. This measuring method has several drawbacks. If the only available measurement is the displacement of the sensor holder, then the force measurement will be altered. Indeed, the displacement of the sensor probe is not equal to the displacement of the sensor holder. Furthermore, a trade-off between the measurement range and the resolution is involved [9]. An increase of the sensor stiffness increases its measurement range at the cost of its resolution. In order to mitigate this drawback, a mechanical structure is used in [10] to change the sensor stiffness when the applied force exceeds a threshold value. To mitigate the first drawback, an additional position sensor can be used such as in [3] for the definition of the deformation/force characteristic of a micro-particle pushed with a force sensor tip. In order to bypass the measurement range/resolution trade-off and the tip position measurement issue, one can design an infinite stiffness sensor, also called a zero displacement sensor.

The working principle of a zero displacement sensor, also referred here as active sensor, is to keep the position of the tip at a fixed value despite of an external applied force. This is feasible thanks to a feedback control that actuate a set of actuators in order to compensate the applied external force. The force measurement is deduced from the actuator voltage or current. Active sensors have also the advantage of being able to provide quantitative force measurement without an accurate calibration of the suspensions. Some of zero displacement sensors have been reported in the literature. In [9] and [11], the sensor is composed of an electrothermal

J. Cailliez, M. Boudaoud, S. Haliyo and S Régnier are with Sorbonne Université, UMR 7222, ISIR, F-75005 Paris, France. A. Mohand Ousaid is with FEMTO-ST Institute, AS2M department, Univ. Bourgogne Franche-Comté / UFC / CNRS UMR-6174/ENSMM, 24, rue Alain Savary, 25000 Besançon, France. A. WEILL–DUFLOS is with McGill University, Centre for Intelligent Machines, 3480 Rue University, Montreal, Quebec H3A 0E9, Canada.E-mail: cailliez(at)isir.upmc.fr, mokrane.boudaoud(at)sorbonne-universite.fr, abdenbi.mohand(at)femto-st.fr, sinan.haliyo(at)sorbonne-universite.fr, stephane.regnier(at)upmc.fr.

position sensor and an electrostatic comb drive actuator. It is an interesting solution, however the main drawback of an electrothermal sensor is that it limits its ability to be used in constrained environments such as vacuum. Furthermore the used a traditional (i.e. not differential) comb drive configuration leads to a quadratic force/voltage relationship that involve control issues for the force measurement. In [12], the zero displacement force sensor includes a piezoresistive position sensor and an additional comb drive actuator to adjust in real time the resonance frequency of the sensor.

This paper deals with the modeling and the experimental characterization of a new active MEMS based force sensor. A 3D representation of the MEMS is shown in Fig. 1. This sensor is designed with a differential comb drive actuator to avoid a nonlinear force/voltage characteristic in the electrical model. It also includes folded-flexure type suspensions to provide a large linear deflection range [13]. This is of importance when the sensor is used in passive mode. A knowledge-based model of the relation probe position/input voltage is proposed. Static and dynamic parameters of the sensor are identified through an experimental analysis. The experimental results are compared with theoretical equations and the limits of the knowledge based model for control purposes are discussed. The linear measurement range of the sensor is about ± 2.45 μN and its resonance frequency is around 2.2 kHz.

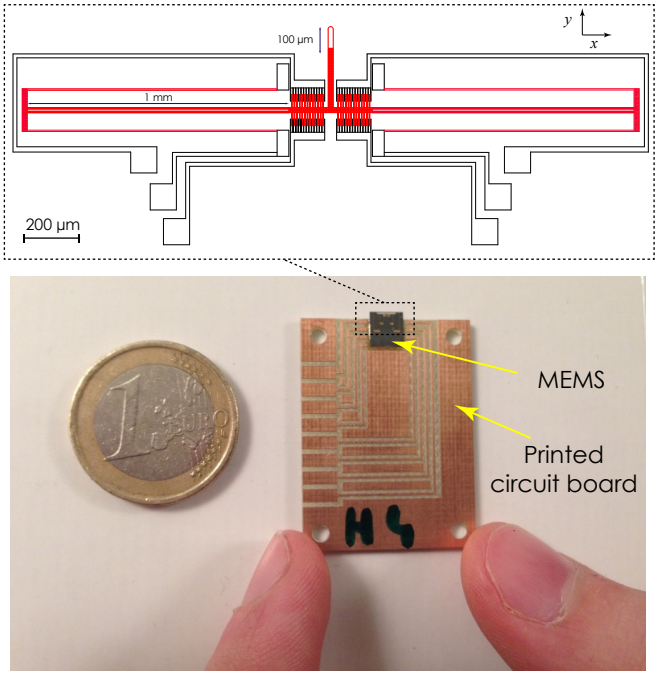

Fig. 2. MEMS based force sensor and enlarged view of the internal structure of the mechanical part. The movable structures are highlighted in red.

A description of the MEMS structure is presented in section II. Section III deals with the electromechanical modeling of the sensor. The model describes the relationship between the sensor probe position and the actuation voltage of the comb drive actuator. The experimental protocol for the dynamic and the static characterization of the sensor is presented in section IV. Experimental data are analyzed and results are followed by several discussions. A conclusion and future perspectives of the work end the paper.

II. Description of the MEMS structure

The sensor is composed of a differential comb-drive actuator, folded-flexure suspensions, a probe and six contact pads for the electrical connections as shown in Fig. 1. It has been monolithically fabricated on a silicon on insulator (SOI) wafer of 30 μm thickness. A wire bonding has been used to connect the contact pads of the MEMS to a printed circuit board (Fig. 2).

The nominal comb drive actuator includes 56 fixed fingers and 52 movable fingers. The gap spacing between the fingers is g = 3.5 μm. The suspensions have 1 mm length and 3.5 μm width. The external part of the probe has a length of 100 μm as shown in Fig. 2. The maximum actuation voltages of the differential comb drive actuator is 70 Volts. The linear displacement range of the probe is about 50 μm. The direction of motion of the probe is the y direction.

III. Dynamic modeling of the MEMS actuator

For control purpose, a dynamic model of the sensor is needed. This section deals with the electromechanical modeling of the transfer between the probe displacement and the input voltages of the differential actuator.

A. Electrical modeling of the differential electrostatic comb drives

Lets consider an elementary pair of fingers of the comb drive actuator as shown in Fig. 3. The movable fingers are represented by the electrode (2). The fixed fingers are represented by the electrodes (1) and (3).

When no voltage is applied, the MEMS is designed so that $y_1 = y_2 = y_0$, where y_1 and y_2 are the overlapping lengths between the electrodes (2) and (1) and the electrodes (2) and (3) respectively (Fig. 3).

Hence, one can write:

$$\begin{cases} y_1 = y_0 - y_e \\ y_2 = y_0 + y_e \end{cases} \quad (1)$$

y_0 is the overlapping length when no voltage is applied and y_e is the displacement of the movable finger in y direction.

The electrostatic force exerted on the movable finger, in y direction, in response to a voltage is equal to the gradient of the electrostatic energy stored by the system.

The stored energy can be expressed as follows :

$$E = \frac{1}{2}\left(C_{12}(V_1 - V_2)^2 + C_{23}(V_2 - V_3)^2 + C_{13}(V_1 - V_3)^2\right) \quad (2)$$

C_{ij} is the capacitance between two electrodes (j) and (i). V_i is the voltage between an electrode (i) and the electrical mass. Here, C_{13} is considered equal to 0.

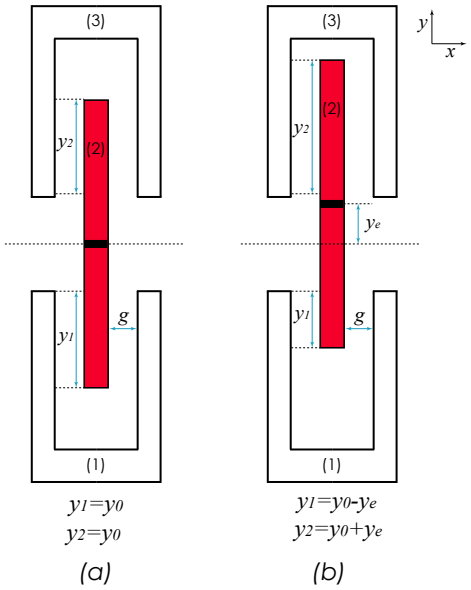

Fig. 3. Simple scheme an elementary pair of fingers in the differential comb drive actuator when the movable fingers are at the initial position $y_e = 0$ (a) and when they are at a position $y_e \neq 0$. The movable fingers are represented by the electrode (2). The fixed fingers are represented by the electrodes (1) and (3).

By neglecting side effects, one can get:

$$\begin{cases} C_{12} = 2(y_0 - y_e)\frac{N\epsilon_0\epsilon_r t}{g} \\ C_{23} = 2(y_0 + y_e)\frac{N\epsilon_0\epsilon_r t}{g} \end{cases} \quad (3)$$

$N = 26$ is the total number of fixed fingers, ϵ_0 is the vacuum permittivity, ϵ_r the relative permittivity and $t = 30\mu m$ the thickness of the electrodes.

Let us now consider the following gain:

$$k_c = \frac{N\epsilon_0\epsilon_r t}{g} \quad (4)$$

The electrostatic force can then be expressed as follows:

$$\begin{aligned} F &= -\frac{\partial E}{\partial y_e} \\ &= k_c((V_1 - V_2)^2 - (V_2 - V_3)^2) \\ &= k_c(V_1^2 + V_2^2 - 2V_1V_2 - V_2^2 - V_3^2 + 2V_3V_2) \end{aligned} \quad (5)$$

By setting $V_1 = -V_3$, which is thereafter used to operate the force sensor, the equation (5) can be simplified as follows:

$$F = 4k_cV_3V_2 \quad (6)$$

Using the numerical value of each parameter of the electrical model, and choosing V_3= 40 V, the relationship between the electrostatic force F that drives the sensor probe and the voltage V_2 is:

$$|F| = 0.3157V_2 \quad [\mu N] \quad (7)$$

The voltages V_1 and V_3 are then set at 40 V and V_2 becomes the only control signal. The linear force/voltage relationship which is one of the main advantage of the differential comb drive actuation is demonstrated.

B. Static mechanical modeling of the suspensions

The aim is to define a knowledge based model of the static force/deflection characteristic for the suspension structure. Let us recall that folded-flexure suspensions are designed for the MEMS sensor (Fig. 1). The bodies C1,C2, and C3 (Fig. 4) are supposed to be infinitely rigid and the flexible structures will be modeled with small displacement theory.

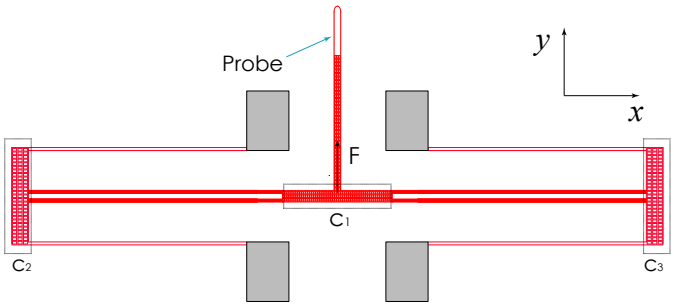

Fig. 4. Schematic representation of the folded-flexure suspensions

Due to the symmetry of the structure, the problem can be reduced by considering the quarter model of the suspensions as shown in Fig. 5. The dimensions of the beam 1 and that of the beam 2 are given is Table I.

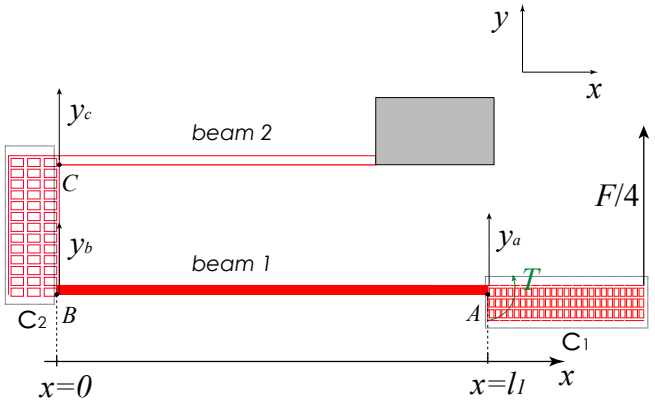

Fig. 5. Quarter model of the suspensions

All the displacements are considered in y direction. The displacement of the rigid body C1 will be supposed equal to the displacement of the point A of the beam 1 relatively to

	width	thickness	length
beam 1	$w = 4.5\ \mu m$	$t = 30\ \mu m$	$l_1 = 1\ mm$
beam 2	$w = 4.5\ \mu m$	$t = 30\ \mu m$	$l_2 = 0.965\ mm$

TABLE I
DIMENSIONS OF THE BEAM 1 AND THE BEAM 2 IN THE SUSPENSION STRUCTURE.

the point B (y_a) plus the displacement of the point C of the beam 2 (y_c). The beam 1 will be supposed clamped at both ends and the beam 2 will be treated as simply clamped. The distance between the points B and C is equal to 18 μm.

The static equilibrium can be defined by the following set of equations:

$$\begin{cases} \{\tau_{beam1\to C2}\}_B = \left\{\begin{array}{c|c} 0 & 0 \\ \frac{F}{4} & 0 \\ 0 & \frac{F\times l_1}{4}+T \end{array}\right\} = \{\tau_{beam1\to C2}\}_C \\ \{\tau_{beam2\to C2}\}_C = -\{\tau_{beam1\to C2}\}_C \\ \{\tau_{C2\to beam1}\}_C = \{\tau_{beam1\to C2}\}_B = \left\{\begin{array}{c|c} 0 & 0 \\ \frac{F}{4} & 0 \\ 0 & \frac{F\times l_1}{4}+T \end{array}\right\} \end{cases} \quad (8)$$

T is the torque. The deflection of the beam 1 at the point of coordinate x will be denoted $Y(x)$.

The bending moment M_f of the beam at a point of distance x is:

$$M_f(x) = T + \frac{F}{4}(l_1 - x) \quad (9)$$

with:

$$\frac{\partial^2 Y}{\partial x^2} = \frac{M_f(x)}{2EI} \quad (10)$$

E is the Young modulus and I is the area moment of inertia.

Considering the initial conditions $Y(0) = 0$ and $\frac{\partial Y}{\partial x}(0) = 0$, the expression of $Y(x)$ can be deduced by a double integration of equation (10) with respect to the variable x.

Therefore:

$$Y(x) = \frac{(T + \frac{F}{4}l_1)x^2 - \frac{F}{12}x^3}{2EI} \quad (11)$$

For $x = l_1$:

$$Y(l_1) = y_a = \frac{Tl_1^2 + \frac{F}{4}l_1^3 - \frac{F}{12}l_1^3}{2EI} \quad (12)$$

By replacing $T = -\frac{F}{8}l_1$ in equation (12), one gets:

$$y_a = \frac{Fl_1^3}{48EI} \quad (13)$$

The beam 2 is considered simply clamped with a torque and a force load at the free end. Its deflection can be considered as the sum of the deflection caused by the torque and that caused by the force. The calculation of these deflections is a standard problem leading to the following analytical formulation:

$$y_c = \frac{Fl_2^3}{12EI} - \frac{Fl_1l_2^2}{16EI} \quad (14)$$

By combining equations (13) and (14), the total displacement of the sensor probe is

$$y_p = \frac{F}{12EI}(\frac{l_1^3}{4} + l_2^3 - \frac{3}{4}l_1l_2^2) \quad (15)$$

The total stiffness k of the suspension structure can then by deduced from the force/displacement relationship:

$$k = \frac{y_p}{F} = \frac{12EI}{\frac{l_1^3}{4} + l_2^3 - \frac{3}{4}l_1l_2^2} \quad (16)$$

Taking into account the dimensions of the MEMS structure and a Young modulus of silicon E = 127 GPa, the model (16) allows obtaining k = 1.37 N/m.

The static force/displacement characteristic of the suspensions has been also analyzed using a computer-aided design (CAD) software. Several finite element analysis with different forces exerted on the probe in y direction have been performed. The operating points have then been fitted to obtain the result of Fig. 6.

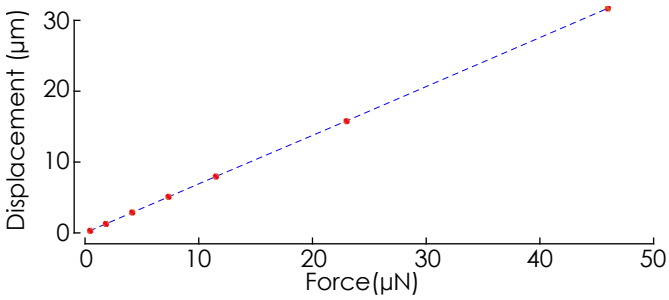

Fig. 6. Static force/displacement finite element characteristic of the suspensions

The finite element analysis leads to a stiffness k=1.451 N/m. The difference between this result and that obtained by the knowledge-based model is equal to 5.58 %. Therefore, the model is considered accurate enough to be used for control design.

C. Electro-mechanical dynamic model of the MEMS

In the previous sections, the electrical force/voltage model and the static mechanical displacement/force model of the MEMS have been obtained knowledge-based model. To extend the model into a dynamic formulation, the damping coefficient μ and the mass m of the movable structure are added here.

The dynamic equation of the movable part of the MEMS can be expressed as follows:

$$m\ddot{y_p} = -ky_p - \mu\dot{y_p} + 4k_cV_3U \quad (17)$$

U=V_2 is the input of the system.

Using the Laplace transform of the equation (17), the transfer function $H(p)$ of the MEMS can be expressed as follows:

$$H(p) = \frac{y_p}{U} = \frac{4k_cV_3}{mp^2 + \mu p + \frac{12EI}{\frac{l_1^3}{4}+l_2^3-\frac{3}{4}l_1l_2^2}} \quad (18)$$

p is the Laplace variable.

IV. Experimental characterization

A. Experimental setup

As shown in Fig. 7, the experimental setup is composed of the MEMS sensor, voltage generators, a Digital Holographic Microscope (DHM) and a vibration isolation table.

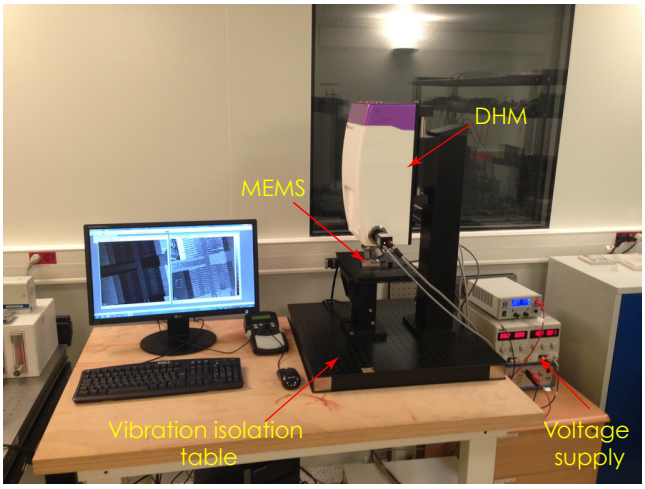

Fig. 7. Experimental setup for the characterization of the MEMS sensor

The DHM is used to measure the displacement of the mobile part of the MEMS in response to a voltage $U = V_2$. A beam of coherent light is emitted and focused on the MEMS. The intensity and phase of the reflected beam are recorded. The phase information is treated to get a 3D real time image of the observed structure.

B. Dynamic characterization of the MEMS actuator

Because of the high resonant frequency of the MEMS, a stroboscopic unit has to be used to be able to track the position of the movable structure. For the experiment, a voltage of 40 V has been chosen for V_3, and the actuator is driven by a square wave $U = V_2$ at 50 Hz. The stroboscope is set to get images at a frequency of 25 kHz. The first problem to solve is that the MEMS is not aligned with the microscope axes. The picture has to be rotated so that the movement direction aligns with that of the images axes. To do so, the user selects 16 points in the image whose coordinates are known a priori. Then, 32 vectors are extracted from the 16 points, and the rotation issue can be expressed as follows:

Let A the matrix containing the vector of coordinates in the image, and B the matrix containing the vector of the a priori coordinates

$$A = \begin{bmatrix} x_{a_1} & y_{a_1} \\ x_{a_2} & y_{a_2} \\ \vdots & \\ x_{a_n} & y_{a_n} \end{bmatrix}, B = \begin{bmatrix} x_{b_1} & y_{b_1} \\ x_{b_2} & y_{b_2} \\ \vdots & \\ x_{b_n} & y_{b_n} \end{bmatrix}$$

such that :

$$B = R \times A \tag{19}$$

This problem can be seen as an overdetermined system of equations. That means that no matrix R is solution of this equation. However several solutions exist to provide a matrix R that minimizes a cost function of $B - RA$. Here, the cost function will be quadratic. The matrix R chosen will be:

$$R = B \times pinv(A) \tag{20}$$

Where $pinv(.)$ represents the moore-penrose pseudoinverse [14].

The rotation angle and scale ratio are extracted from R. The image if first rotated, missing pixels are recovered by a linear interpolation between neighboring points. The pixels intensities are then summed vertically. The result is shown in Fig. 9 for one position of the MEMS probe and in Fig. 8 for several positions.

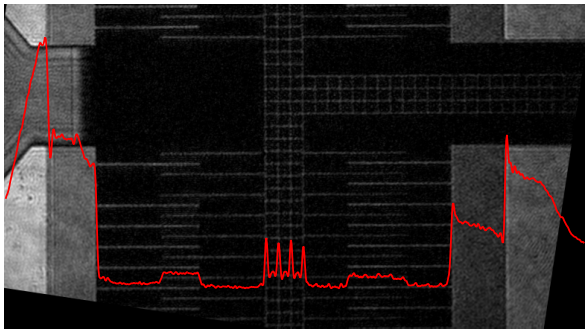

Fig. 8. Top view of the MEMS with the DHM and example of curve showing vertical sum of pixels for a fixed position of the probe.

In the region of interest (ROI), there is a clean pattern. Therefore, the probe position y_p if defined as follows:

$$y_p = \frac{\sum_{ROI} xI(x)}{\sum_{ROI} I(x)} - x_0 \tag{21}$$

where $I(x)$ is the vertical sum of the intensities on pixel r.

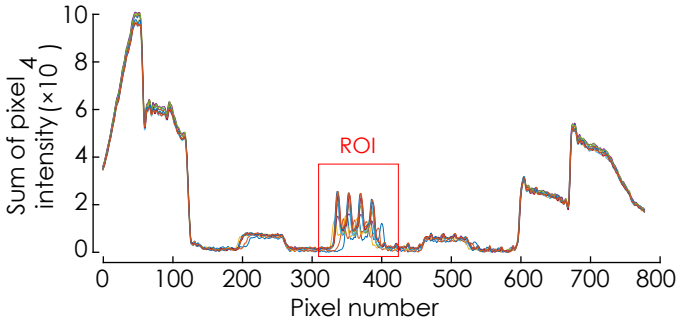

Fig. 9. Vertical sum of pixels for different values of displacements of the sensor probe

This method has been used to measure the step response of the MEMS probe experimentally. Fig. 10 shows the experimental step response of the system for a U = 4.5 Volts step input. These signals has been used to identify a second order model $H_i(p)$ describing the dynamic behavior of the MEMS. The step response of the model for a 4.5 Volts step input is also shown in Fig. 10.

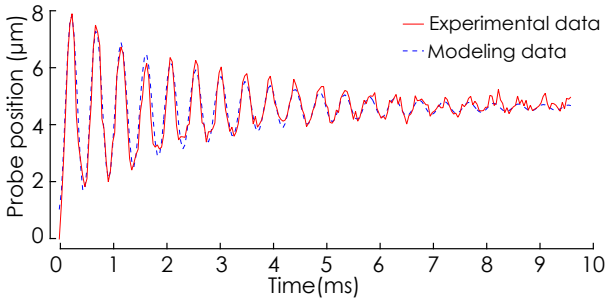

Fig. 10. Experimental and simulation step response of the MEMS sensor for a U = 4.5 Volts step input

The identified transfer function $H_i(p)$ is:

$$H_i(p) = \frac{1.684 \times 10^8}{p^2 + 774.6p + 1.818 \times 10^8} \tag{22}$$

Its input and output are expressed in Volts and μm respectively. The resonant frequency of this model is 2.2 kHz. This value is coherent with the one obtained through the finite element analysis of the MEMS. The mass and the damping can be identified from (22).

C. Static characterization of the MEMS actuator

The MEMS static characterization is essential in order to check the system linearity. To do so, the setup described in section IV-B is used. The system input is chosen to be sine wave with low frequency equal to 5 Hz. The position is recorded and plotted with respect to the input voltage. Result is shown in Fig. 11.

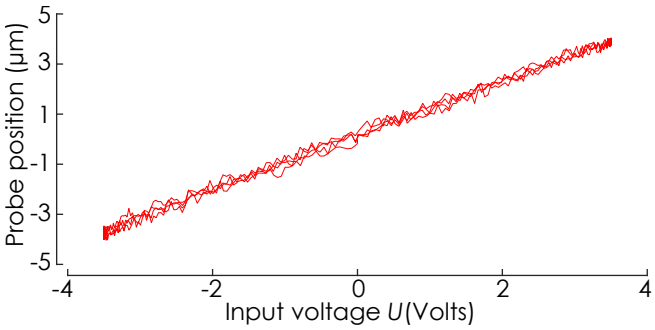

Fig. 11. Experimental static characteristic of the MEMS sensor

This curve can be modeled by first order polynomial. The experimental static gain of the MEMS is equal to 1.0854 μm/V. The static gain deduced from the fitted transfer function is 0.9263 μm/V. The non linearity error is lower than 0.4 μm. This error is in part due to the image noise.

V. Conclusion

Based on a differential comb-drive actuator and a folded-flexure suspension, a new MEMS force sensor is proposed in this paper. It allows, unlike passive sensors, the measurement of forces in a wide range with nanoNewton resolutions. By design, its suspension is arranged to constrain the sensor probe within a single direction. Whilst, the differential actuator is chosen to provide a linear force/voltage relationship where force and probe position are independent. In view of using a zero displacement principle (balance principle), a control oriented electromechanical model is driven. Preliminary experimental characterization validates this model in static and dynamic operating modes using a stroboscopic measurement system. The sensor shows a promising potential with a resonant frequency of 2.2 kHz, and a static passive measurement range of $\pm$ 2.45 μN. This result is the first step toward a new generation of active force sensors able to capture high dynamic forces within a large range of measurement. Future wok will focus on the feedback control of the sensor in order to take advantage of zero displacement sensing. This step will consist to design a controller in order to generate an opposite balance force to cancel the action of the interaction forces. The measurement will be related directly to the balanced force which keeps the probe at equilibrium position.

References

[1] N. Chaillet and S.Rgnier. Microrobotics for micromanipulation, isbn: 9781848211865. 2013.

[2] Steven J. Koch, Gayle E. Thayer, Alex D. Corwin, and Maarten P. de Boer. Micromachined piconewton force sensor for biophysics investigations. *Applied Physics Letters*, 89(17):173901, 2006.

[3] S. Kohyama, H. Takahashi, S. Yoshida, H. Onoe, K. H. Shoji, T. Tsukagoshi, T. Takahata, and I. Shimoyama. Mems force and displacement sensor for measuring spring constant of hydrogel microparticles. In *International Conference on Micro Electro Mechanical Systems (MEMS)*, 2017.

[4] Tao Mei, Wen J Li, Yu Ge, Yong Chen, Lin Ni, and Ming Ho Chan. An integrated mems three-dimensional tactile sensor with large force range. *Sensors and Actuators A: Physical*, 80(2):155–162, 2000.

[5] C. A. Gutierrez, C. McCarty, B. Kim, M. Pahwa, and E. Meng. An implantable all-parylene liquid-impedance based mems force sensor. In *2010 IEEE 23rd International Conference on Micro Electro Mechanical Systems (MEMS)*, pages 600–603, Jan 2010.

[6] Felix Beyeler, Simon Muntwyler, Zoltn Nagy, Chauncey Graetzel, Matthias Moser, and Brad Nelson. Design and calibration of a mems sensor for measuring the force and torque acting on a magnetic microrobot. 18:025004, 12 2007.

[7] M. Boudaoud, Y. Haddab, and Y. Le Gorrec. Modeling and optimal force control of a nonlinear electrostatic microgripper. *IEEE/ASME Transactions on Mechatronics*, 18(3):1130–1139, June 2013.

[8] W. Gao, L. Zhao, Z. Jiang, Y. Xia, X. Guo, Z. Zhao, Y. Zhao, and D. Sun. A novel mems force sensor based on laterally movable gate array field effect transistor(lmgafet). In *International Conference on Nano/Micro Engineered and Molecular Systems (NEMS)*, 2017.

[9] M Bulut Coskun, Steven Moore, SO Reza Moheimani, Adrian Neild, and Tuncay Alan. Zero displacement microelectromechanical force sensor using feedback control. *Applied Physics Letters*, 104(15):153502, 2014.

[10] W. Chen, J. Jiang, J. Liu, and W. Chen. A mems based sensor for large scale force measurement. In *2013 IEEE/ASME International Conference on Advanced Intelligent Mechatronics*, pages 1278–1283, July 2013.

[11] Steven Ian Moore, M Bulut Coskun, Tuncay Alan, Adrian Neild, and SOR Moheimani. Feedback-controlled mems force sensor for characterization of microcantilevers. *Journal of Microelectromechanical Systems*, 24(4):1092–1101, 2015.

[12] M. Maroufi, H. Alemansour, and S. O. R. Moheimani. A closed-loop mems force sensor with adjustable stiffness. In *2017 IEEE Conference on Control Technology and Applications (CCTA)*, pages 438–443, Aug 2017.

[13] A. W. Groeneveld R. Legtenberg and M. Elwenspoek. Comb-drive actuators for large displacements. *J. Micromech. Microeng*, 6(3):320329, 1996.

[14] Pierre Courrieu. Fast computation of moore-penrose inverse matrices. *CoRR*, abs/0804.4809, 2008.